




Surfactant-free carbon black@graphene conductive ink for flexible electronics

Xinbin Qiu¹, Xiaomin Zhao¹, Feixiang Liu¹, Songlin Chen¹, Jianfeng Xu¹, and Guohua Chen^{1,*} 

¹ College of Materials Science and Engineering, Huaqiao University, Xiamen 361021, Fujian, China

Received: 15 March 2019

Accepted: 7 May 2019

Published online:

13 May 2019

© Springer Science+Business Media, LLC, part of Springer Nature 2019

ABSTRACT

The capabilities of conductive ink with both excellent conductivity and flexibility properties are extremely important for the construction of next-generation flexible electronic devices. However, the development of an appropriate ink possessing high conductivity and good dispersity remains a big challenge for ink-jet printing. Here, an original synthesis method of surfactant-free carbon black@graphene (CB@rGO) conductive ink is reported via freeze-drying process and reduction in p-phenylenediamine. The CB@rGO ink unambiguously displays a well-defined and smooth morphology, extremely the CB@rGO conductive particles showing good stability in many solvents. The CB@rGO film exhibited outstanding flexibility which is showed by the durable conductivity after bending 1000 times. Furthermore, it has an excellent conductivity of $714 \pm 90 \text{ S m}^{-1}$, and these data increased to $5091 \pm 200 \text{ S m}^{-1}$ after the high temperature post-processing increased by 198% compared to the traditional rGO film. Notably, the absence of surfactant in conductive fillers' dispersing process contributed to the high conductivity of CB@rGO ink compared with the traditional ones.

Introduction

The development of conductive inks for flexible, portable and printable radio frequency identification devices (RFID), electrodes, energy devices, sensors, and other electronic devices has attracted tremendous attention in recent years [1–6]. Depositing circuit on a flexible board or designing self-supporting flexible conductive film is an effective way for the fabrication of high-density foldable electronic devices

[1, 7]. In the past decades, a numerous types of materials such as inorganic nanoparticles, metal nanowires, conducting polymers and carbon materials have been used in conductive ink for flexible electronics [8, 9]. However, many challenges for these conductive inks are limiting their development of industrial products. For instance, metal conductive inks are not stable in environmentally friendly solvents which usually need organic addition agents and the high annealing temperature [10]. In addition,

Address correspondence to E-mail: hdcgh@hqu.edu.cn

another drawback of metal conductive ink is the consumption of expensive metallic nanoparticles.

One possible approach to solve this problem is the utilization of highly conductive carbon nanomaterials [2, 8, 11]. To date, graphene conductive ink has attracted considerable interest from the viewpoint of the fabrication of flexible electronic devices, due to its excellent conductivity, film-forming property and mechanical flexibility [2, 7, 12–14]. Currently, graphene inks using water as solvent show low conductivity owing to the addition of insulated surfactant [15–17]. Graphene inks using un-eco-friendly organic solvents (e.g., N-methylpyrrolidone (NMP) and dimethylformamide (DMF)) have low viscosity (< 2 cP) and low concentration (< 0.1 mg mL⁻¹), suggesting that several tens of print passes are required to obtain conductive films which is low efficiency for the printed electronic technique [17–19]. Large-scale fabrication of hydrophilic graphene oxide (GO) and reduced graphene oxide (rGO) ink has been reported. The conductivity of self-supporting printed GO film can be promoted after the oxygen-containing functional groups being removed by chemical reduction [20–24]. The graphene in rGO inks formed by chemical reduction methods from GO can be modified simultaneously with different functional groups (sulfonic acid group, phenol groups, alkoxy group). The surface functionalization of graphene is necessary for both the modification of their dispersing properties and the acquisition of new characteristics [25–27]. Owing to the electrical pathway effect of graphene and the decreased contact resistance of graphene junctions by Ag nanoparticles, the Ag/graphene conductive ink possesses excellent conductivity and some flexibility [28]. However, before long, silver migration can easily occur from silver loads on graphene system and the graphene/Ag structure is destroyed in the end because there is no extra force to support this structure. There still remain many challenges that need to be overcome before graphene inks can actually become industrial products, especially in designing flexible electronics. Therefore, environment-friendly, high concentrations and surfactant-free graphene conductive inks are meaningful for the development of flexible electronics.

In this study, a well-dispersed, stable, surfactant-free and high conductive CB@rGO ink for the fabrication of flexible electronics was developed successfully. The CB@rGO conductive ink showed excellent

dispersion that can be dispersed steadily with high concentration in various solvents for months in the absence of surfactant. The film prepared by CB@rGO ink showed excellent flexibility that it can be retained most of its conductivity after thousands of folds. The uniquely dispersibility and conductivity of CB@rGO ink endowed the constructed flexible electronics with durability, and most importantly, it provided many alternative solvents for the next-generation printing ink and avoided the use of high toxic organic solvents. We utilized ammonia PPD as reductant to reduce GO. The PPD oxidation products (OPPD) can interact with rGO by strong π - π stacking interactions and repelling π - π stacking interactions between rGO sheets during chemical reduction. In addition, the adherent carbon black (CB) particles between rGO sheets achieve the deaggregation of rGO sheets and decreasing the contact resistance between rGO sheets. Therefore, we believed that the synthesized CB@rGO conductive ink could be utilized as printable environmentally friendly conductive ink for flexible electronics.

Experiment section

Chemicals and materials

Nature graphite was purchased from Xiamen Knano Graphene Technology Co., Ltd. CB was purchased from Tianyi Century chemical Co., Ltd. The chemicals include p-phenylenediamine (PPD), ethanol (ET), ethylene glycol (EG), isopropanol (IPA), DMF, NMP provided by Aladdin Industrial Co., Ltd. The water used in all procedures was deionized water. All these materials and chemicals were used as-received without further purifications.

Synthesis of CB@GO conductive precursors

Initially, GO was synthesized from natural flake graphite (8000 mesh) via a modified Hummers method [20, 21]. Then, GO aqueous dispersion (2 mg/mL) was obtained after ultrasonic processing. An amount of CB particles (0.05 g, 0.1 g, 0.2 g, 0.4 g, 0.8 g) which was wetted by ethanol was mixed with 100 mL of the GO dispersion by high-frequency ultra-sounding. The carbon black@graphene oxide (CB@GO) precursor including freeze-drying CB@GO (FCB@GO), 80 °C drying CB@GO (DCB@GO) and

without drying CB@GO (NCB@GO) was obtained by three different methods of freeze drying, 80 °C drying and without drying, respectively. FCB@GO was prepared with different mass ratios of CB/GO (4/1, 2/1, 1/1, 1/2 and 1/4). The mass ratio of CB/GO for DCB@GO and NCB@GO was prepared as 1/1.

Synthesis of CB@rGO conductive inks

0.4 g FCB@GO, DCB@GO, NCB@GO conductive precursor was sonicated in 100 mL EG for 5 min. Successively, an amount of amino reductant PPD was dissolved into conductive precursor dispersion and GO was chemically reduced in 90 °C water bath for 24 h. The CB@rGO conductive materials were obtained after filtering and washing by EG for three times. At last, CB@rGO conductive inks were prepared by dispersing CB@rGO conductive materials into different solvents (water, EA, EG, IPA, DMF, NMP) via ultrasonic process. High reduction degree FCB@GO (HFCB@rGO), high reduction degree DCB@GO (HDCB@rGO) and high reduction degree NCB@GO (HNCB@rGO) represent three kinds of conductive inks which obtained from the FCB@GO, DCB@GO and NCB@GO precursors with high reduction degree when the PPD usage was 4 g. Low reduction degree FCB@GO (LFCB@rGO) was the conductive inks from the FCB@GO precursors with low reduction degree when the PPD usage was 0.4 g.

Preparation of HFCB@rGO conductive films

The HFCB@rGO conductive film was prepared by spin coating on glass substrate under 80 °C drying. The annealing HFCB@rGO (AHFCB@rGO) film was prepared by blade coating on ceramic substrate under 400 °C annealing for 2 h in argon atmosphere. The rolling AHFCB@rGO (RAHFCB@rGO) film was prepared by rolling the AHFCB@rGO film with a glass tube.

Characterizations

The micromorphology of the conductive particles was investigated by the field-emission scanning electron microscopy (FESEM, NJSM-6700F, JEOL, Tokyo, Japan). The powder X-ray diffraction (XRD, D8-Advance instrument, Bruker AXS, America) was operated with Cu K α radiation at a scan rate (2θ) of 5° min⁻¹ with an accelerating voltage of 40 kV. The

Raman spectra were recorded from 500 to 3500 cm⁻¹ on a Raman spectrometer (Raman, LABRAM, HJY, France). The Fourier transform infrared spectra were collected from 1800 to 1000 cm⁻¹ using a RQUINOX55 spectrometer (FTIR, 8400S, Shimadzu, Japan). The chemical composition of conductive materials was investigated by X-ray photoelectron spectroscopy (XPS) using an ESCALab250 electron spectrometer (Thermo Scientific Corporation) with monochromatic 150 W Al K α radiation. The sheet resistance (Rs) was measured on the digital four probe meter (SZ82, Suzhou Telecommunication Instrument, China). Thermogravimetric analysis (TGA) was carried on DTG-60H (Shimadzu, Japan) from room temperature to 800 °C in air at a heating rate of 10 °C·min⁻¹.

Results and discussion

The characterization of CB@rGO conductive particles

The preparing route of HFCB@rGO conductive ink is described schematically in Fig. 1a. The SEM images of FCB@GO precursor and HFCB@rGO particle are shown in Fig. 1b, c, respectively. Figure 1d shows the nitrogen element mapping image of HFCB@rGO. The XRD diffraction curves of GO, CB, FCB@GO and HFCB@rGO are shown in Fig. 1e. The SEM and film images HFCB@rGO, HDCB@rGO, HNCB@rGO conductive films are shown in Fig. 1f, g and h, respectively. The SEM image of synthesized HFCB@GO with different CB/GO ratios (4/1, 1/1 and 1/4) conductive precursor particles is shown in Fig. S1 (a, b, c), respectively.

As shown in Fig. 1b, CB particles were uniformly distributed between the GO sheets on the structure of FCB@GO precursor. FCB@GO exhibited the stacked structure with ~ 4.7 μm in diameter, which is shown in Fig. S2(a–c). During the chemical reduction process, GO sheets were reduced to wrinkled rGO sheets. The as-prepared HFCB@rGO showed similarly spherical structure particles with ~ 4.9 μm in diameter (Fig. 1c and Fig. S2(d–e)). No CB particle was observed on the shell of the spherical structure, indicating that they were encapsulated inside the rGO sheets. Hence, a core–shell structure was proposed for the HFCB@rGO, which had a core of layered rGO sheets and CB particles and a shell of

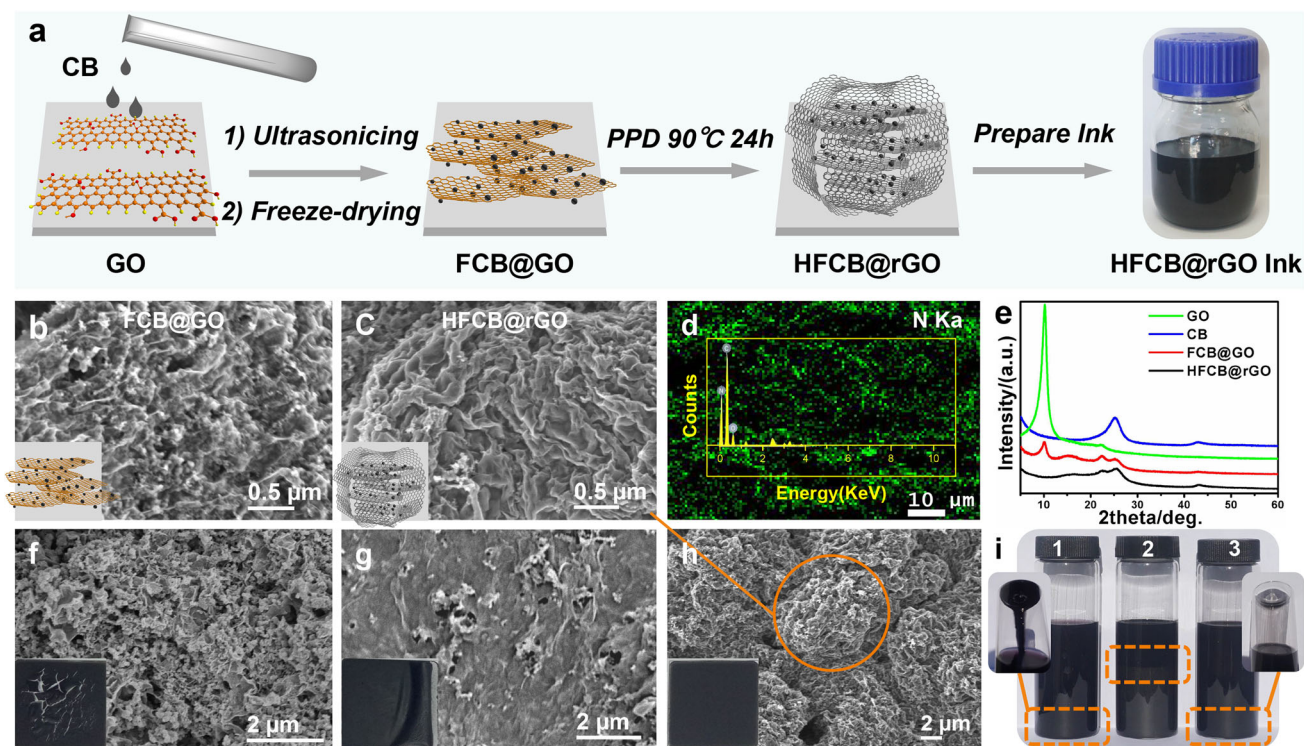


Figure 1 a Synthesis diagram of HFCB@rGO conductive ink. b, c SEM image of synthesized FCB@GO conductive precursor particles and HFCB@rGO conductive particles. d SEM element mapping and energy-disperse spectroscopy (EDS) curves of the HFCB@rGO materials. e XRD for HFCB@rGO nanoparticles to demonstrate the reduction in GO. f–h SEM image of synthesized

HFCB@rGO, HDCB@rGO, HNCB@rGO conductive particles, respectively. (The insets are HNCB@rGO, HDCB@rGO, HFCB@rGO film.) i Photographs of HNCB@rGO (1), HDCB@rGO (2), HFCB@rGO (3) conductive particles dispersed in EG with a concentration of $20 \text{ mg}\cdot\text{mL}^{-1}$ were taken after standing for 2 months.

wrinkled rGO sheets (Fig. 1a). In Fig. 1d, the nitrogen element mapping distribution was well dispersed on the sphere of HFCB@rGO, suggesting that rGO sheets were coated uniformly on the shell due to that the nitrogen element was solo from PPD structure. In Fig. 1e, the GO materials showed the characteristic diffraction peaks at 10.3° which corresponds to the interlayer spacing (8.60 \AA), the CB particles showed the characteristic diffraction peaks at 25.6° , 42.9° , and the FCB@GO precursor materials showed the characteristic diffraction peaks of CB particle at 25.6° , 42.9° and that of GO sheets at 10.3° . After the chemical reduction, the HFCB@rGO materials showed the characteristic diffraction peak of CB particles at 25.6° , 42.9° and that of rGO sheets at $2\theta = 22.8^\circ$ which corresponding to an interlayer spacing of about 3.91 \AA , and the interlayer spacing (3.91 \AA) of rGO is larger than that of graphite (3.36 \AA) [29, 30]. The presence of defects and the OPPD which attached to the rGO sheets surface by π - π conjugate action can prevent

perfect π - π stacking of graphene sheets, which expending the interlayer space [31].

In this work, freeze-drying process was found to be one important step for the formation of FCB@GO precursor. The HNCB@rGO and HDCB@rGO conductive particles synthesized via two different drying process of drying at 80°C and without drying, respectively, were studied in comparison with FCB@GO. In Fig. 1f, HNCB@rGO conductive ink film was cracked and the phase of CB and rGO was separated on the SEM image. In Fig. 1g, HDCB@rGO conductive ink film was non-uniform. The rGO sheets were stacked and CB particles were covered by overlapping rGO sheets in a microscale. However, the HFCB@rGO showed a core-shell structure as we mentioned at above and its conductive ink film was very uniform (Fig. 1h), suggesting that the freeze-drying process played an important role in the formation of HFCB@rGO. It is because that the FCB@GO conductive precursor was formed slowly at a low temperature (-10°C) and low atmospheric pressure

(0.35 mbar) for 48 h. Therefore, there is enough time for porous carbon black particles sticking to GO sheets due to the strong capillary force in low pressure. The increasing surface energy prompted GO sheets to aggregate under the freeze-drying process, whereas the uniform distribution of CB particles on GO sheets can hinder the aggregation of GO due to the increasing capillarity of porous CB particles in FCB@GO structure. Overall, the strong capillarity between GO sheets and porous CB supported the formation of the HFCB@rGO structure and prevented the phase migration phenomenon when HFCB@rGO was dispersed in solvents.

In the next reduction procedure, rGO sheets which on the surface of CB@GO precursor begin to shrink and generated wrinkle, and then, the rGO sheets stuck to the FCB@GO precursor particles in order to resist the reduction in surface tension; gradually, the FCB@GO precursor particles were surrounded by rGO sheets completely and the HFCB@rGO particles were formed in the end [32, 33]. To understand the structure of HFCB@rGO particle, SEM analysis of HFCB@rGO is performed (Fig. 1c, h), the as-obtained HFCB@rGO is nearly spherical structure particles, and the wrinkles of rGO sheets are observed on the surface of HFCB@rGO particles. Figure 1i shows the dispersion of HNCB@rGO, HDCB@rGO, HFCB@rGO in EG, in the absence of surfactant. It was found that HFCB@rGO conductive ink displays better stability than HDCB@rGO and HNCB@rGO conductive ink, the phase migration phenomenon occurs in HNCB@rGO conductive ink and there is a lot of precipitation in the bottom of HDCB@rGO conductive ink. The HFCB@rGO conductive material can disperse in many solvents for a long time, and the dispersion performance in other solvents is shown in Fig. S3.

The reduction mechanism of rGO

The chemical reduction in GO by means of PPD is illustrated in Fig. 2a. In the case of a small amount of reductant (mass ratio of PPD/GO was 1/1), the amino group of PPD firstly reacted with the carboxyl group on GO, resulting in the amide bonds between PPD and GO. In addition, there was a ring-opening reaction between amino and epoxy group that would be happen after the amidation in the first step. In this case, the LFCB@rGO material can disperse steadily in most solvents due to the introduction of amino

group. When adding an excess of reductant ($M_{PPD}/M_{GO} = 10$), most of the oxygen functional groups were removed, and a series of reactions generated large amount of hydrophilic OPPD. So HFCB@rGO ink displays not only excellent dispersing performance due to strong conjugate effect between OPPD and the rGO sheets on particle surface, but also high conductivity due to maximum reduction in GO sheets. The images of LFCB@rGO and HFCB@rGO inks with a concentration of 20 mg mL^{-1} in Fig. 2d were taken after standing for 2 months.

The resulting HFCB@rGO material was characterized by Raman spectra, FTIR spectra and XPS spectra, all of which confirmed that the reduction in graphene had taken place. Figure 2b shows the Raman spectrum for FCB@GO, LFCB@rGO and HFCB@rGO materials, and all their Raman spectra of the conductive material exhibited the characteristic D and G bands at 1339 and 1584 cm^{-1} , respectively. In general, the area ratio I_D/I_G of D and G peaks was considered to be related to the average size of the sp^2 domain. The higher Raman I_D/I_G means the smaller sp^2 domain size and the more sp^2 domains [30, 34–36]. The calculated I_D/I_G ratio of FCB@GO, LFCB@rGO and HFCB@rGO materials is 0.95, 1.02 and 1.13, respectively, suggesting the number of sp^2 domains following the sequence: HFCB@rGO > LFCB@rGO > FCB@GO. Further insights on chemical changes caused by PPD were shown in FTIR spectra (Fig. 2c). The FTIR peaks of FCB@GO at 1207 cm^{-1} , 1384 cm^{-1} and 3434 cm^{-1} assigning to the epoxide (C–O–C), C=O and hydroxy (–OH) groups, respectively, demonstrated that the conductive precursor FCB@GO contained a large number of oxygen-containing functional groups, such as epoxy group, ketone group, carboxyl group and hydroxyl group [37–39]. The characteristic peak of C–N at 1117 cm^{-1} indicated that the amido reaction occurred between PPD and GO in the FTIR spectrum of LFCB@rGO and HFCB@rGO. Compared with the FTIR spectrum of FCB@GO, those of LFCB@rGO and HFCB@rGO did not show obvious difference owing to the existing of CB.

The XPS spectrum (Fig. 2e–g) showed evidences that C–N was generated and oxygen-containing bonds reduced in LFCB@rGO and HFCB@rGO compared with FCB@GO. Besides, the HFCB@rGO showed more nitrogen content (12.55%), while less oxygen (5.12%) than those of LFCB@rGO (9.32% and 8.79%, respectively), which indicated the further ring-

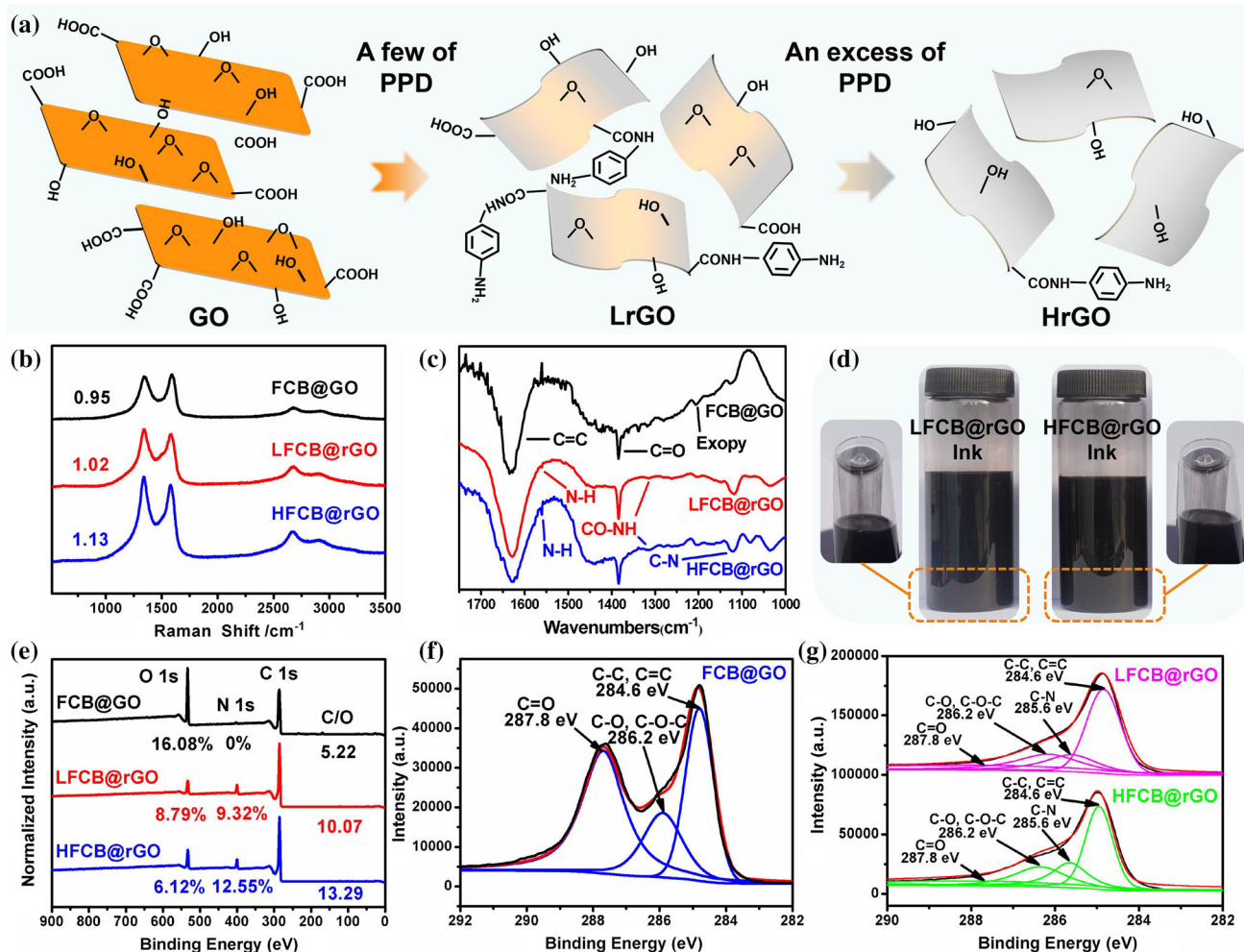


Figure 2 a Reduction mechanism schematic of GO in the HFCB@rGO conductive material. **b** Raman spectra for FCB@GO, LFCB@rGO and HFCB@rGO materials to demonstrate the reduction in GO. **c** FTIR spectra for FCB@GO, LFCB@rGO and HFCB@rGO materials to be clarified the changes of functional groups after chemical reduction. **d** Photographs of LFCB@rGO and HFCB@rGO ink were taken

opening reaction occurred under the high proportion of PPD reductant. To clarified successfully chemical reduction in FCB@GO precursor, the high-resolution C1s spectra for FCB@GO, LFCB@rGO and HFCB@rGO materials were compared, as shown in Fig. 2f, g. The C1s spectra of FCB@GO indicated a considerable degree of oxidation with three different peaks at 284.6, 286.2 and 287.8 eV, corresponding to C-C/C=C in aromatic rings, C-O-C/C-O (epoxide and alkoxy groups) and C=O (carboxyl and ketone groups), respectively [30, 40]. The spectrum of LFCB@rGO and HFCB@rGO showed that there is a new peak for C-N at 285.6 eV, which demonstrated

after standing for 2 month and with a concentration of 20 mg·mL⁻¹. **e** XPS spectra for FCB@GO, LFCB@rGO and HFCB@rGO materials to demonstrate the existence of nitrogen after chemical reduction. **f**, **g** High-resolution C1s spectra for FCB@GO, LFCB@rGO and HFCB@rGO materials, respectively, to demonstrate the occurrence of nitrogen-containing functional groups.

the reduction in GO by PPD. In addition, the spectra of HFCB@rGO showed a stronger peak intensity at 284.6 eV (C=C) and at 285.6 eV (C-N) than LFCB@rGO, which indicated that the graphene network of C=C bonds was further restored in HFCB@rGO.

The conductivity of CB@rGO ink films

Figure 3a shows the RAHFCB@rGO conductive film fabrication route from HFCB@rGO ink in which HFCB@rGO particles were dispersed in the EG solvent, then spin coating on the ceramic substrate to

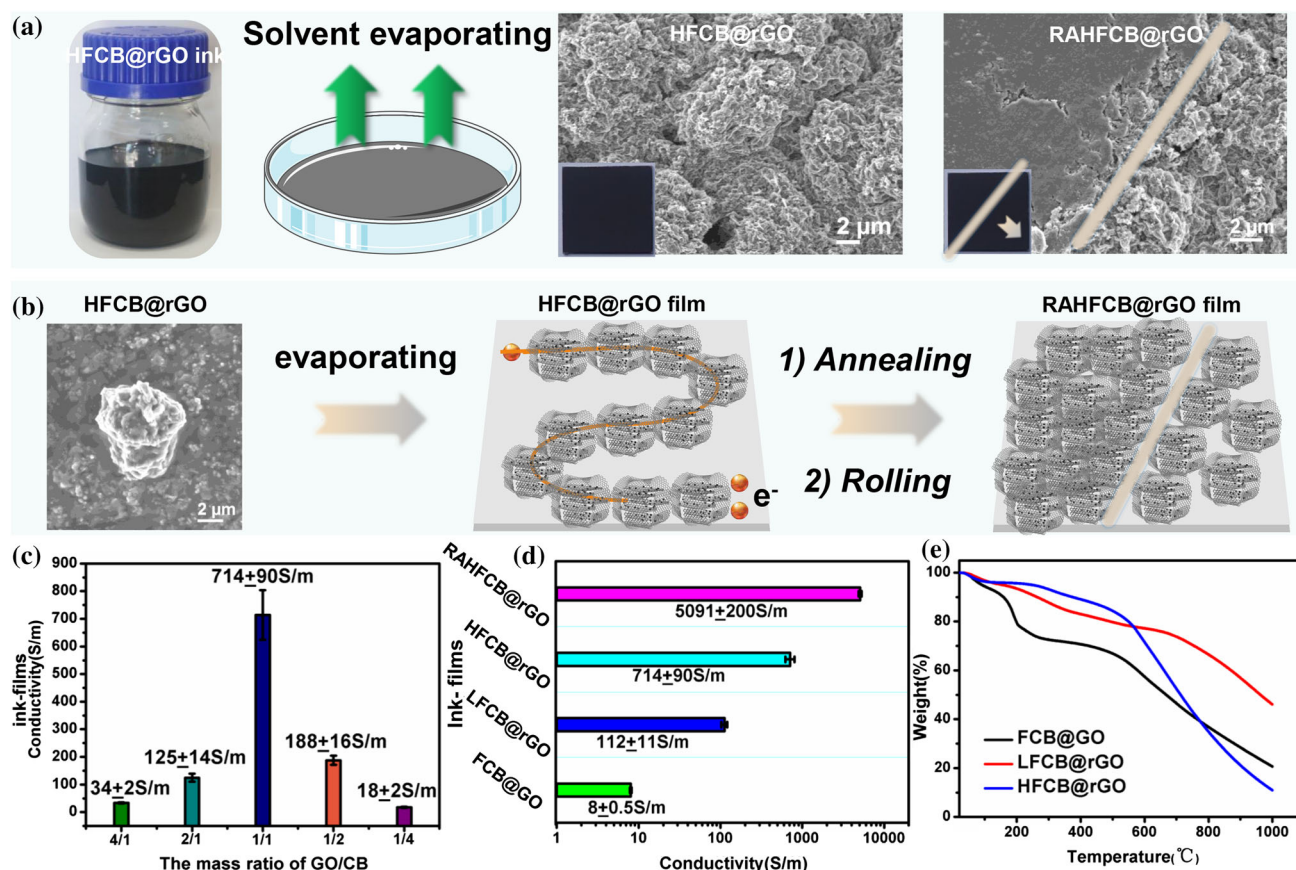


Figure 3 a Preparation process of RAHFCB@rGO conductive material. (The insets are AHFCB@rGO film and RAHFCB@rGO film.) b The formation process scheme of the conductive pathway model (graphene–carbon black–graphene) of RAHFCB@rGO

material. c Electrical conductivity of the different mass ratio of HFCB@rGO films. d Electrical conductivity of conductive films with different treatments. e TGA curves in the air of: FCB@GO, LFCB@rGO and HFCB@rGO materials.

make complete uniform film, followed dried in oven at 80 °C for 5 h to remove solvent. The success of the uniform film fabrication depends on the uniform nearly spherical structure of the conductive particles, and the wrinkles of rGO sheets on the surface of conductive particles cause corrugated particles tend to unite. To increase the conductivity of HFCB@rGO particles, post-processing methods, such as thermal annealing or compression rolling, can be employed [41–44]. In particular, thermal annealing is known to be a very efficient method to improve the conductivity of GO, and the high-temperature annealing could remove the residual oxygen-containing functional groups (main hydroxy) of rGO sheets in HFCB@rGO material completely, and then, it obtained AHFCB@rGO material. At the following procedure, compression rolling was employed to improve the compactness of AHFCB@rGO film material. RAHFCB@rGO material possessed

smoother surface than AHFCB@rGO. Figure 3b demonstrates the formation process of the conductive pathway model (graphene–carbon black–graphene) of RAHFCB@rGO material in detail.

The impact of GO/CB mass ratio on the conductivity of HFCB@rGO conductive ink was studied with different ratios of 4/1, 2/1, 1/1, 0.5/1 and 0.25/1. As shown in Fig. 3c, the conductivity of HFCB@rGO(1/1) ink was 714.29 S m⁻¹ which was the highest than those with other GO/CB mass ratios. The conductivities of HFCB@rGO(1/4) and HFCB@rGO(4/1) inks were 34.76 S m⁻¹ and 18.23 S m⁻¹, respectively, which were much lower than that of HFCB@rGO(1/1). On one side, rGO sheets preferred to agglomerate to form large precursor particles when GO/CB mass ratio was high during the reduction process of GO, resulting in poor dispersibility of HFCB@rGO in solvent. On the other side, the low conductivity of CB particles caused that

of HFCB@rGO(4/1) when the GO/CB mass ratio was low. Obviously, a good matching relation of HFCB@rGO(1/1) ink film between rGO sheets and carbon black nanoparticles make him endowed with high conductivity. Meanwhile, the AHFCB@rGO material was treated at 400 °C and was naturally more conductive than the HFCB@rGO material which treated by chemical reduced only (Fig. 3d). But, unfortunately, high-temperature annealing of conductive particles results in layer expansion between carbon black particles and rGO sheets that along with the decrease in conductivity. So, it is necessary for AHFCB@rGO material to compression rolling, and the structural integrity of the AHFCB@rGO film is restored by compression rolling resulting. Thus, RAHFCB@rGO film with smooth surface, high density and high conductivity ($5091 \pm 200 \text{ S m}^{-1}$) was obtained, which increased by 198% in conductivity compared to the traditional rGO film ($2420 \pm 200 \text{ S m}^{-1}$) [45], and 960% higher than that of carbon black film. Unfortunately, the rigid ceramic substrate and the high-temperature annealing treatment limited the application of RAHFCB@rGO film in flexible electronics field.

Figure 3e shows the TGA curves of FCB@GO, LFCB@rGO and HFCB@rGO materials in air atmosphere. All these materials exhibited about 5% weight loss attributed to the removal of solvents below 100 °C. LFCB@rGO and HFCB@rGO materials did not show significant mass loss between 100 °C and 300 °C, indicating that the sample did not contain a significant amount of thermally labile oxygen functional groups. In contrast, FCB@GO materials exhibited 20% weight loss attributed to the removal of thermally labile oxygen functional groups between 100 °C and 300 °C. Actually, there was still a 15% weight loss in HFCB@rGO materials material below 600 °C, most likely due to loss of stable oxygen-containing functional groups and small amount of solvent. All of the above materials showed significant mass loss above 600 °C, and it could be due to pyrolysis of the carbon skeleton, because the oxygen in air contributes to pyrolysis of the carbon skeleton which breakdown at 800 °C under inert gas [46–48].

The performance of flexible conductive paper electronics

Figure 4a shows the printing patterns of HFCB@rGO ink via brush printing for flexible electronic. Various

predefined patterns such as aligned stripe and the HQU logo were prepared by one-time brush printing of HFCB@rGO ink on a cellulose paper (Fig. 4a, b). A light bulb was able to turn on attributing to the conductivity of stripe or HQU logo printing pattern via applying an extra 5.0 V potential (Fig. 4c), showing that the printing patterns of HFCB@rGO had enough conductivity (714.29 S m^{-1}) for the electronics. The stripe pattern was twined around the cylindrical tube or a finger (Fig. 4d), which was able to be maintained for a long time. The above results revealed that the HFCB@rGO ink film would have satisfactory electrical conductivity and high-dimensional stability during the usage. Hence, the impact of bending act on the conductivity of the stripe patterns was studied targeting to see whether HFCB@rGO ink was suitable for flexible electronic, considering its two mentioned advantages. As shown in Fig. 4e, the conductivity of carbon black ink film dramatically decreased during bending 100 times, and completely lost the conductivity due to the broke of conductive path after bending 500 times. The reduction in conductivity of CB ink film was caused by the generated crack and the low adhesive ability of CB ink on the paper during the bending behavior. However, the HFCB@rGO ink film showed almost a constant conductivity after 10 times bending. The reduction in conductivity was kept within 15% after 1000 times bending.

The good mechanical flexibility of HFCB@rGO ink film benefits from its special structure. A shell of wrinkled rGO sheets of HFCB@rGO ink particles provides a special meshing effect and frictional resistance between HFCB@rGO particles, which reduces the generation and the propagation of crack. Meanwhile, a core of layered rGO sheets and inserted CB particles of HFCB@rGO particles is a good cushion structure, which could absorb partial stress shear. In addition, the good adhesion between ink film and cellulose paper substrate ensures that the conductive path is not easy to be peeled off from substrate. Through the fundamental mechanisms above, the HFCB@rGO ink film exhibited high conductivity retention. Thus, the flexible test demonstrated that the good adhesion and the special folding-resistant structure of HFCB@rGO film, suggesting that it would be an alternative material for the flexible electronics by a high-efficiency printing process.

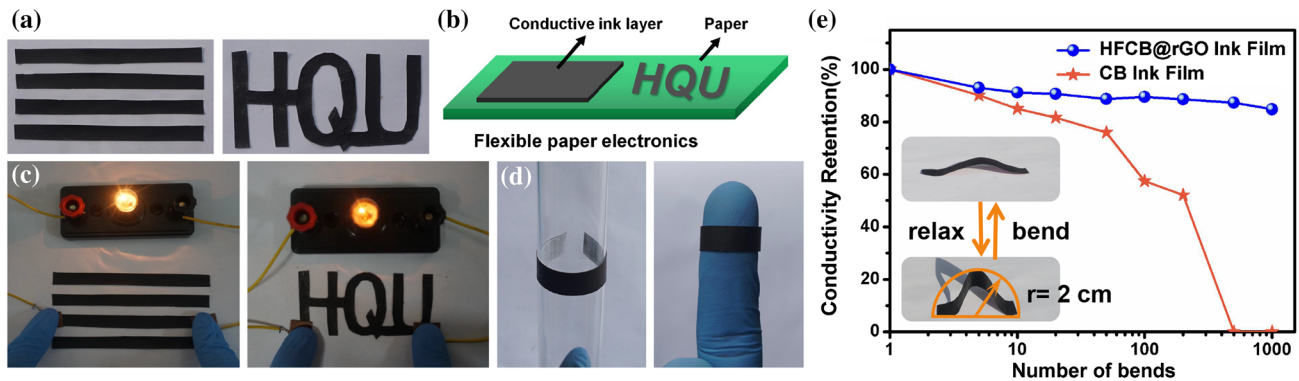


Figure 4 a, b Fabrication of HFCB@rGO ink-based paper electronics in different patterns by brush-printing method. c Photograph showed a light bulb connected by HFCB@rGO ink coated paper. d The flexible test of electronic paper.

Conclusions

We had successfully developed a surfactant-free HFCB@rGO conductive ink with high viscosity, and conductivity via an innovative strategy. This conductive ink exhibited a well-defined and smooth morphology, extremely showed good stability in many solvents such as EA, EG, IPA, DMF and NMP. This ink showed good adaptability to conventional coating/printing processes. Notably, the carbon black particles played an important role in the process by means of prevented the agglomeration of graphene and reduced contact resistance between rGO sheets. The HFCB@rGO(1/1) ink film had an optimal conductivity of $714 \pm 90 \text{ S m}^{-1}$, and these data increased to $5091 \pm 200 \text{ S m}^{-1}$ after the post-processing of high-temperature annealing and compression rolling, which increased by 198% compared to the traditional RGO film. The high conductivity is explainable by the absence of surfactant during the preparation. Furthermore, the HFCB@rGO ink film still showed the durable conductivity after bending 1000 times, exhibited both outstanding conductivity and flexibility. These performances showed that HFCB@rGO ink had a potential application in the field of flexible electronics. Moreover, this surfactant-free and environmentally friendly ink which using EG as solvent provided an efficient and environmentally friendly method to fabricate conductive ink. Overall, it is believed that the developed HFCB@rGO ink has great potential for designing flexible electronic devices in the further, and we also expected that this synthesis of HFCB@rGO ink will start a new pathway

e Electrical characteristics of HFCB@rGO ink-based electronic paper during bending and relaxing deformation for 1000 times. (The bending radius of flexible electronics is 2 cm. The flexible experiment was conducted in outward bending.).

for adapting the macroscopic usages of graphene nanomaterials in senior and energy fields.

Acknowledgments

This work was financially supported by National Natural Science Foundation of China (51373059, 51603076), Science and Technology Projects in Fujian province (2017H2001, 2018H6012, 2018H0019), and the Research Center of Graphene Powder & Composites of Fujian Province and Development and Reform Commission of Fujian Province.

Compliance with ethical standards

Conflicts of interest All the authors declare that they have no conflict of interest.

Electronic supplementary material: The online version of this article (<https://doi.org/10.1007/s10853-019-03687-2>) contains supplementary material, which is available to authorized users.

References

- [1] Scidà A, Haque S, Treossi E, Robinson A, Smerzi S, Ravasi S, Borini S, Palermo S (2018) Application of graphene-based flexible antennas in consumer electronic devices. *Mater Today* 21:223–230
- [2] Cheng C, Zhang JG, Li S, Xia Y, Nie CX, Shi ZQ, Cuellar-Camacho JL, Ma N, Haag R (2017) A water-processable and bioactive multivalent graphene nanoink for highly flexible bioelectronic films and nanofibers. *Adv Mater* 30:1705452

- [3] Choudhary N, Li C, Moore J, Nagaiah N, Zhai L, Jung Y, Thomas J (2017) Asymmetric supercapacitor electrodes and devices. *Adv Mater* 29:1605336
- [4] Wu HJ, Wu GL, Ren YY, Yang L, Wang LD, Li XH (2015) $\text{Co}^{2+}/\text{Co}^{3+}$ ratio dependence of electromagnetic wave absorption in hierarchical $\text{NiCo}_2\text{O}_4\text{-CoNiO}_2$ hybrids. *J Mater Chem C* 3:7677–7690
- [5] Jia ZR, Lin KJ, Wu GL, Xing H, Wu HJ (2018) Recent progresses of high-temperature microwave-absorbing materials. *NANO* 13:1830005
- [6] Bonaccorso F, Bartolotta A, Coleman JN, Backes C (2016) 2D-crystal-based functional inks. *Adv Mater* 28:6136–6166
- [7] Lee CL, Chen CH, Chen CW (2013) Graphene nanosheets as ink particles for inkjet printing on flexible board. *Chem Eng J* 230:296–302
- [8] Li LH, Guo YZ, Zhang XY, Song YL (2014) Inkjet-printed highly conductive transparent patterns with water based Ag-doped graphene. *J Mater Chem A* 2:19095–19101
- [9] Jia ZR, Lan D, Lin KJ, Qin M, Kou KC, Wu GL, Wu HJ (2018) Progress in low-frequency microwave absorbing materials. *J Mater Sci-Mater El* 29:17122–17136
- [10] Zhu J, Hersam MC (2017) Assembly and electronic applications of colloidal nanomaterials. *Adv Mater* 29:1603895
- [11] Majee S, Liu C, Wu B, Zhang SL, Zhang ZB (2017) Ink-jet printed highly conductive pristine graphene patterns achieved with water-based ink and aqueous doping processing. *Carbon* 114:77–83
- [12] Geim AK, Novoselov KS (2007) Graphene calling. *Nat Mater* 6:169
- [13] Chen J, Shepherd RL, Razal JM, Huang X, Zhang WM, Zhao J, Harris AT, Wang S, Minett AI, Zhang H (2007) Scalable solid-template reduction for designed reduced graphene oxide architectures. *ACS Appl Mater Interfaces* 5:7676–7681
- [14] Park S, Lee KS, Bozoklu G, Cai WW, Nguye ST, Ruoff RS (2008) Graphene oxide papers modified by divalent ions-enhancing mechanical properties via chemical cross-linking. *ACS Nano* 2:572–578
- [15] Han X, Chen Y, Zhu H, Preston C, Wan J, Fang Z, Hu L (2013) Scalable, printable, surfactant-free graphene ink directly from graphite. *Nanotechnology* 24:205304
- [16] Zhang ZC, Sun JJ, Lai C, Wang Q, Hu CG (2017) High-yield ball-milling synthesis of extremely concentrated and highly conductive graphene nanoplatelet inks for rapid surface coating of diverse substrates. *Carbon* 120:411–418
- [17] Li JT, Ye F, Vaziri S, Muhammed M, Lemme MC, Ostling M (2013) Efficient inkjet printing of graphene. *Adv Mater* 25:3985–3992
- [18] Majee S, Song M, Zhang SL, Zhang ZB (2016) Scalable inkjet printing of shear-exfoliated graphene transparent conductive films. *Carbon* 102:51–57
- [19] Karagiannidis PG, Hodge SA, Lombardi L, Tomarchio F, Decorde N, Milana S, Goykhman I, Su Y, Mesite SV, Johnstone DN, Leary RK, Midgley PA, Pugno NM, Torrisil F, Ferrari AC (2017) Microfluidization of graphite and formulation of graphene-based conductive inks. *ACS Nano* 11:2742–2755
- [20] Marcano DC, Kosynkin DV, Berlin JM, Sinitskii A, Sun Z, Slesarev A, Alemany LB, Lu W, Tour JM (2010) Improved synthesis of graphene oxide. *ACS Nano* 4:4806–4814
- [21] Pei S, Cheng HM (2012) The reduction of graphene oxide. *Carbon* 50:3210–3228
- [22] Wang M, Duong LD, Oh JS, Mai NT, Kim S, Hong S, Hwang T, Lee Y, Nam JD (2014) Large-area, conductive and flexible reduced graphene oxide (RGO) membrane fabricated by electrophoretic deposition (EPD). *ACS Appl Mater Interfaces* 6:1747–1753
- [23] Wei D, Li HW, Han DX, Zhang QX, Niu L, Yang HF, Bower C, Andrew P, Ryhanen T (2011) Properties of graphene inks stabilized by different functional groups. *Nanotechnology* 22:1–7
- [24] Karousis N, Economopoulos SP, Sarantopoulou E, Tagmatarchis N (2012) Porphyrin counter anion in imidazolium-modified graphene-oxide. *Carbon* 48:854–860
- [25] Park S, An J, Jung I, Piner RD, An SJ, Li X, Velamakann A, Ruoff RS (2009) Colloidal suspensions of highly reduced graphene oxide in a wide variety of organic solvents. *Nano Lett* 9:1593–1597
- [26] Rogala M, Wlasny I, Dabrowski P, Kowalczyk PJ, Busiakiewicz A, Kozlowski W (2015) Graphene oxide overprints for flexible and transparent electronics. *Appl Phys Lett* 106:041901
- [27] Lin J, Chen D, Dong J, Chen G (2015) Preparation of polyvinylpyrrolidone-decorated hydrophilic graphene via in situ ball milling. *J Mater Sci* 50:8057–8063. <https://doi.org/10.1007/s10853-015-9373-6>
- [28] Xu LY, Yang GY, Jing HY, Wei J, Han YD (2014) Ag-graphene hybrid conductive ink for writing electronics. *Nanotechnology* 25:055201
- [29] Zhou M, Tian T, Li XF, Sun XD, Zhang J, Cui P, Tang J, Qin LC (2014) Production of graphene by liquid-phase exfoliation of intercalated graphite. *Int J Electrochemical SC* 9:810–820
- [30] He DF, Shen LM, Zhang XY, Wang YF, Bao NZ (2014) An efficient and eco-friendly solution-chemical route for preparation of ultrastable reduced graphene oxide suspensions. *AIChE J* 60:2757–2764

- [31] Szabo T, Berkesi O, Dekany I (2015) Drift study of deuterium-exchanged graphite oxide. *Carbon* 43:3186–3189
- [32] Chen Y, Zhang X, Yu P, Ma YW (2019) Stable dispersions of graphene and highly conducting graphene films: a new approach to creating colloids of graphene monolayers. *Chem Commun* 30:4527–4529
- [33] Jeon IY, Shin YR, Sohn GJ, Choi HJ, Bae SY, Mahmood J, Jung SM, Seo JM, Kim MJ, Chang DW, Dai L, Baek JB (2012) Edge-carboxylated graphene nanosheets via ball milling. *P Natl Acad Sci USA* 109:5588–5593
- [34] Jiang J, Liu FX, Zhuang KY, Chen DQ, Chen GH (2017) Composites of epoxy/graphene-modified-diamond filler show enhanced thermal conductivity and high electrical insulation. *Rsc Adv* 7:40761–40766
- [35] He H, Gao C (2010) General approach to individually dispersed, highly soluble, and conductive graphene nanosheets functionalized by nitrene chemistry. *Chem Mater* 22:5054–5064
- [36] Abdolhosseinzadeh S, Asgharzadeh H, Kim HS (2015) Fast and fully-scalable synthesis of reduced graphene oxide. *Sci Rep-UK* 5:10160
- [37] Eigler S, Hu Y, Ishii Y, Andreas H (2013) Controlled functionalization of graphene oxide with sodium azide. *Nanoscale* 5:12136–12139
- [38] Jia ZR, Gao ZG, Lan D, Cheng YH, Wu GR, Wu HJ (2018) Effects of filler loading and surface modification on electrical and thermal properties of epoxy/montmorillonite composite. *Chin Phys B* 27:117806
- [39] Lan D, Qin M, Yang R, Chen S, Wu H, Fan Y, Zhang F (2019) Facile synthesis of hierarchical chrysanthemum-like copper cobaltate-copper oxide composites for enhanced microwave absorption performance. *J Colloid Interf Sci* 533:481–491
- [40] Faghani A, Donskyi IS, Gholami MF, Ziem B, Lippitz A, Unger WES, Böttcher C, Rabe JP, Haag R, Adeli M (2017) Controlled covalent functionalization of thermally reduced graphene oxide to generate defined bifunctional 2D nanomaterials. *Angew Chem* 56:2619–2723
- [41] Paton KR, Varrla E, Backes C, Smith RJ, UmarKhan O'Neill A, Boland C, Lotya M et al (2014) Scalable production of large quantities of defect-free few-layer graphene by shear exfoliation in liquids. *Nat Mater* 13:624–630
- [42] Arapov K, Bex G, Hendriks R, Rubingh E, Abbel R, With GD, Friedrich H (2016) Conductivity enhancement of binder-based graphene inks by photonic annealing and subsequent compression rolling. *Adv Eng Mater* 18:1234–1239
- [43] Peng L, Xu Z, Liu Z, Guo Y, Li P, Gao C (2017) Ultrahigh thermal conductive yet superflexible graphene films. *Adv Mater* 29:1–8
- [44] Kölpin N, Wegener M, Teuber E, Polster S, Frey L, Roosen A (2013) Conceptual design of nano-particulate ITO inks for inkjet printing of electron devices. *J Mater Sci* 48:1623–1631
- [45] Stankovich S, Dikin DA, Piner RD, Kohlhaas KA, Kleinhammes A, Jia Y, Wu Y, Nguyen ST, Ruoff RS (2007) Synthesis of graphene-based nanosheets via chemical reduction of exfoliated graphite oxide. *Carbon* 45:1558–1565
- [46] Wu HJ, Qu SH, Lin KJ, Qing YC, Wang LD, Fan YC, Fu QH, Zhang HL (2018) Enhanced low-frequency microwave absorbing property of SCFs@TiO₂ composite. *Powder Technol* 333:153–159
- [47] Wu HJ, Wu GL, Wang LD (2015) Peculiar porous α -Fe₂O₃, γ -Fe₂O₃ and Fe₃O₄ nanospheres: facile synthesis and electromagnetic properties. *Powder Technol* 269:443–451
- [48] Su R, Sun W, Tian C, Chen GH (2015) An edge-decorated submicron reduced graphite oxide nanoflakes and its composites with carbon nanotubes for transparent conducting films. *Rsc Adv* 5:46785–46789

Publisher's Note Springer Nature remains neutral with regard to jurisdictional claims in published maps and institutional affiliations.